Utrecht University

Bachelor Thesis

Physics & Astronomy

Feasibility Study of Σ_c-Baryon Reconstruction Using the ALICE Detector at CERN LHC

Author
Loek Meijers
Student Number
4244788

Supervisor
Dr. Alessandro Grelli
Co-Supervisor
Syaefudin Jaelani MSc

January 16, 2019

Universiteit Utrecht

Abstract

A recent ALICE paper pointed out that the charmed baryon-to-meson (Λ_c/D^0) production ratio in pp and p-Pb collisions deviates about a factor of 5 from that same ratio in ee and ep collisions at lower center of mass energies. This deviation breaks the expected universality of the fragmentation function. A large theoretical effort is ongoing to understand the result of the ALICE paper. One of the proposed ideas is that the offset in the ratio could be caused by a difference in the Σ_c production rate in pp and p-Pb collisions as opposed to ee and ep collisions. Σ_c decays into a Λ_c and a π with a probability of 100%. It was impossible to disentangle Λ_c coming directly from charm quarks from those coming from Σ_c-decay in the ALICE data. The measured Λ_c/D^0-ratio thus contains Λ_c from both mentioned sources. For this thesis, Pythia8 was used to study the kinematics of the $\Sigma_c \to \Lambda_c\ \pi$ decay in order to set selection criteria for the reconstruction of Σ_c in real data. The selection cuts proposed in this thesis were used to attempt the reconstruction of Σ_c in pp data at $\sqrt{s} = 5$ TeV. In the Σ_c p_t-bin [8,12] GeV/c from the ALICE data, a hint of a signal peak was found. This peak appears at the expected location of the invariant mass difference, which is promising for further research into the value of the Λ_c/D^0-ratio determined in the ALICE paper.

Contents

1 Introduction

In an ALICE collaboration paper published at the end of 2017[1], the Λ_c^+/D^0 production ratio was calculated from ALICE datasets of pp and p-Pb collisions at center of mass energies $\sqrt{s} = 7$ TeV and $\sqrt{s_{NN}} = 5.02$ TeV respectively. The value that was found deviates from earlier determinations. These earlier determinations were the experimental results of other experiments, done with different collision systems at different center of mass energies.

Table 1: Different findings of the Λ_c^+/D^0 production ratio [1]

	$\Lambda_c^+/D^0 \pm$ stat. $\pm$ syst.	System	$\sqrt{s}$ (GeV)	Notes
ALICE	$0.543 \pm 0.061 \pm 0.160$	pp	7000	
ALICE	$0.602 \pm 0.060^{+0.159}_{-0.087}$	p-Pb	5020	
CLEO	$0.199 \pm 0.021 \pm 0.019$	ee	10.55	
ARGUS	0.127 ± 0.031	ee	10.55	
LEP average	$0.113 \pm 0.013 \pm 0.006$	ee	91.2	
ZEUS DIS	$0.124 \pm 0.034^{+0.025}_{-0.022}$	ep	320	$1 < Q^2 < 1000$ GeV, $p_t < 10$ GeV/c, $0.02 < \lvert y \rvert < 0.7$
ZEUS γp, HERA I	$0.220 \pm 0.035^{+0.027}_{-0.037}$	ep	320	$130 < W < 300$GeV, $Q^2 < 1$GeV^2 $p_t > 3.8$GeV/c, $\lvert\eta\rvert < 1.6$
ZEUS γp, HERA II	$0.107 \pm 0.018^{+0.009}_{-0.014}$	ep	320	$130 < W < 300$GeV, $Q^2 < 1$GeV^2 $p_t > 3.8$GeV/c, $\lvert\eta\rvert < 1.6$

As can be seen in table 1 above, the baryon-to-meson-ratios found at ALICE differ significantly from the values which were determined earlier. The mean of the ratios found at ALICE is 0.573, while the mean of the values of the ratio determined earlier trough ee end ep collisions is 0.148. This finding is interesting to the field of particle physics as a whole, because it indicates that the expected universality of the fragmentation ratios is broken at the TeV energy-scale. Secondly, such a high ratio points to an "over production" of Λ_c with respect to present scientific literature. Once the ALICE results on Λ_c production (combined with the production results of D-mesons) will be used to calculate the total charm cross-section, the result may point to a significant deviation from the expectations of perturbative Quantum ChromoDynamics (pQCD).

Shortly after the publication of the ALICE values of the baryon-to-meson ratio, it was proposed that the differences in the ratios could be caused by a change in the production rate of Σ_c-Baryons. This production rate could be different in pp and p-Pb collisions at the mentioned energies, as opposed to the types of collisions investigated at different energies in previous experiments. This could be the cause of the offset in the ratio, because the decay channel $\Sigma_c \rightarrow \Lambda_c\ \pi$ is a strong decay. This results in the mean lifetime of the decaying particle being much less than for weak decays. We do not have the ability to separate prompt Λ_c from Λ_c coming from the strong Σ_c-decay, because the Σ_c decays into $\Lambda_c\ \pi$ almost instantaneously. Therefore, the Λ_c from Σ_c-decays are not displaced from the primary collision vertex, mimicking the behavior of the Λ_c baryons coming directly from charm fragmentation (prompt Λ_c). As a result, all Λ_c coming from the Σ_c decay-channel enter into the measured charmed baryon-to-meson ratio Λ_c/D^0.

The scope of this thesis will be to study the kinematics of the $\Sigma_c \rightarrow \Lambda_c\ \pi$ decay in order to set selection criteria for the reconstruction of the Σ_c-baryon. The reconstruction will be attempted in the data sets collected by the ALICE collaboration at CERN Large Hadron Collider. In case reconstruction of the Σ_c-baryon is possible, the ratio $(\Lambda_c(c) - \Lambda_c(\Sigma_c))/\mathrm{D}^0$ could be investegated. This way it could be checked what role Λ_c-baryons from Σ_c decays play in the deviation from universality found by ALICE. The sample used consists of 900 M pp collisions at $\sqrt{s} = 5$ TeV collected during run II of the Large Hadron Collider.

The above leads to the formulation of the following research question:

Is it feasible to perform the reconstruction of the Σ_c-baryon with the ALICE detector at CERN Large Hadron Collider?

2 Theory

2.1 The Standard Model

The model along which lines most of physics is understood, carries the name 'standard model'[2]. This model gives an explanation for 3 of the 4 fundamental interactions in nature: the strong, weak and electromagnetic interactions. Physicists hope to be able to implement the gravitational interaction into the standard model in the future, but no one has succeeded to do this as of yet. The basic concept of this model is that the three forces it describes are a result of the interactions between elementary particles. The particles which undergo these interactions can be grouped into quarks, leptons and bosons. The constituents of the standard model can be seen below in figure 18

Particles which are made out of quarks are called hadrons. Hadrons can be subdivided into mesons and baryons, where mesons are made out of a quark and an anti-quark, and baryons are made out of three quarks or three anti-quarks.

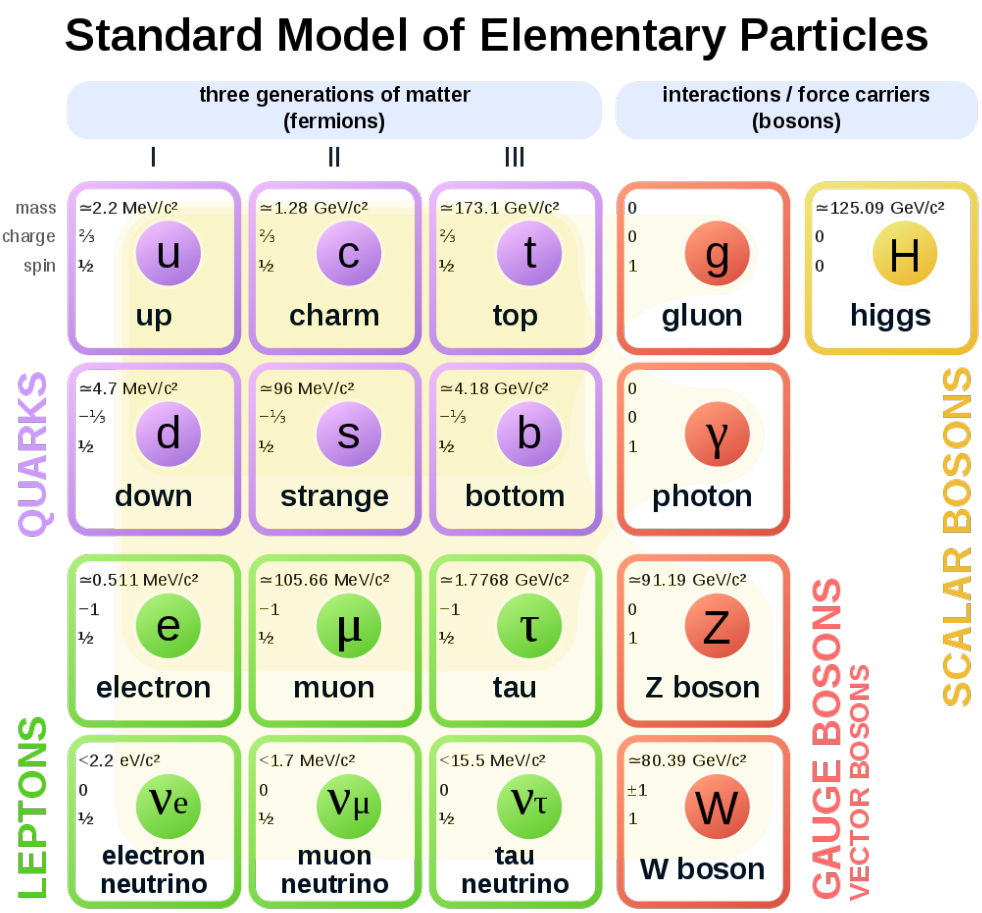

Figure 1: Constituents of the standard model[3] Note that for each lepton and quark, an anti-particle exists with the same mass and opposite charge (if charge is relevant). bosons are their own anti-particles.

2.2 Definitions and quantities

2.2.1 Transverse momentum

A quantity often used within particle physics is the transverse momentum. The transverse momentum is defined as the components of momentum which are perpendicular to the beam axis in a collider experiment. If we take the beam axis as the z-axis, the transverse momentum is given by

$$p_t = \sqrt{p_x^2 + p_y^2}. \tag{1}$$

2.2.2 Invariant mass

An understanding of the way the invariant mass of particles which are not directly detected by the ALICE detector is determined, is essential for this thesis. Within special relativity, the mass-momentum relationship is given by

$$E = \sqrt{p^2c^2 + m_0^2c^4}. \text{ [2]} \tag{2}$$

Given that this quantity is conserved, and taking into account that both the energy and the momentum of particles can be measured by the ALICE detector, the invariant mass of the mother particle of two tracks can be reconstructed by rewriting to

$$m_0 = \sqrt{(\frac{E_1 + E_2}{c^2})^2 - (\frac{p_1 + p_2}{c})^2}. \tag{3}$$

2.2.3 Center of mass energy

The center of mass energy, represented by $\sqrt{s}$, is the energy at which two particles are being collided into each other seen from the center of mass of the two particles. In particle physics, four-momenta (p^μ) are often used. These four-momenta consist of four components. The first contains the energy of a particle divided by c, and the next three contain the three-momentum of a particle, or just 'the momentum':

$$p^\mu = \begin{bmatrix} E/c \\ \mathbf{p} \end{bmatrix}. \tag{4}$$

Multiplication of this four-vector with itself gives the square of the first component, minus the square of the last three components. When particles collide, we can express their center of mass energy in the lorentz-invariant form

$$\sqrt{s} = \sqrt{p^\mu p_\mu} = \sqrt{E^2/c^2 - \mathbf{p}^2}. \text{[4]} \tag{5}$$

Filling in the energies (E_1, E_2) and momenta (p_1, p_2) of two colliding particles of rest masses m_1 and m_2, and using that $|\mathbf{p}| = p$, we get

$$\begin{aligned} s &= \frac{(E_1 + E_2)^2}{c^2} - (\mathbf{p}_1 + \mathbf{p}_2)^2 \\ &= \frac{E_1^2}{c^2} + \frac{E_2^2}{c^2} + \frac{E_1E_2}{c^2} - \mathbf{p}_1^2 - \mathbf{p}_2^2 - \mathbf{p}_1 \cdot \mathbf{p}_2 \\ &= m_1^2c^2 + m_2^2c^2 + \frac{E_1E_2}{c^2} - p_1p_2\cos\theta, \end{aligned} \tag{6}$$

which in the case of identical particles of mass m_1 colliding head-on with equal momentum p_1 becomes

$$s = 2m_1^2c^2 + \frac{E_1^2}{c^2} + p_1^2$$

2.2.4 Pseudo-rapidity

Another quantity often appearing in particle physics is the pseudo-rapidity of a detector. This quantity paremetrizes the azimuthal angle coverage of a detector (θ), which is the angle starting at the plane perpendicular to the beam direction increasing in positive direction. Pseudo-rapidity is given by

$$\eta = -\ln(\tan(\theta/2))[5] \tag{7}$$

The pseudo-rapidity coverage of a detector is often given as $|\eta|$, implying that the coverage goes as far in the positive direction as it does in the negative direction.

2.2.5 Significance

To be able to state anything about whether a peak in a fit to a distribution is there due to random background fluctuations, or whether it actually means something, a quantity called the *significance* is introduced. To be able to observe a particle trough reconstruction, physicists make fits to histograms obtained from data. To make a fit, a signal function and a background function are introduced. The combination of both functions, called the *total* function should give the best fit to the datapoints. The parameters used for the fit function which resulted in the best fit can be extracted. Since the mean (μ) and the standard deviation (σ) of the signal function are parameters of the total function, they can be extracted. The significance is obtained by taking the integral of the used signal function over the range $[\mu - 3\sigma, \mu + 3\sigma]$ (S). Subsequently an integral of the used background function has to be taken over the same range (B). The significance α is then given by

$$\alpha = \frac{\mathrm{S}}{\sqrt{\mathrm{S} + \mathrm{B}}}. \tag{8}$$

It was agreed upon that a peak with $\alpha > 3$ can be called an *observation*, and that a peak with $\alpha > 5$ can be called a *discovery*. Peaks with these values of significance are classified as such because they correspond to 3σ and 5σ deviations from the assumed background shape (according to Gaussian statistics).

2.3 The ALICE detector

The ALICE[6] apparatus consists of several sub-detectors. The ones most important for this thesis are briefly discussed below. The placing of the sub-detectors with respect to the the ALICE apparatus can be seen in the appendix.

2.3.1 Inner Tracking System (ITS)

The main purpose of the ITS is the determination of the primary vertex location. The resolution of this determination depends on the charged particle density coming from the observed collision. With increasing momentum, the resolution will increase due to the reduction of material budget and misalignment effects. The resolution for the primary vertex position as a function of charged-particle density in pp collisions is given in figure 2.

The ITS is capable reconstructing the decay vertex of resonances that travel as few as 100 μm before decay as well as enhancing the resolution of momentum measurements executed by the Time Projection Chamber. The ITS consists of silicon pixel detectors in its innermost 2 layers, silicon drift detectors in the next 2 layers, and finally 2 layers of silicon micro-strip detectors. The phase-space covered by the ITS in the analyzed data sets is $|\eta| < 0.9$[7].

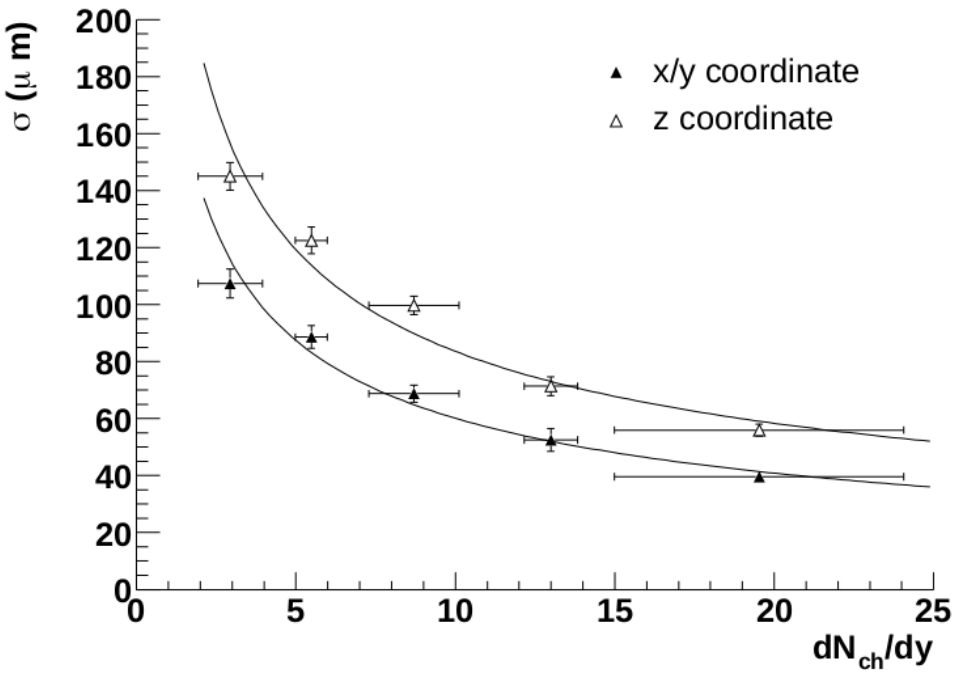

Figure 2: Primary vertex resolution as a function of charged-particle density.[7]

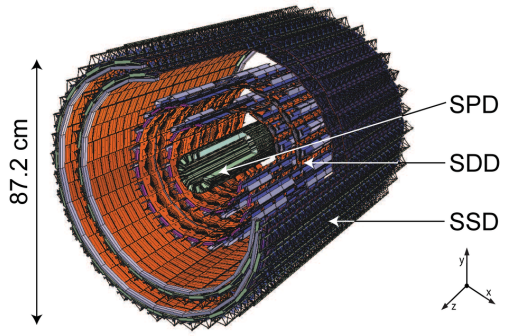

Figure 3: Schematic View of the ALICE ITS[8]

2.3.2 Time Projection Chamber (TPC)

The TPC is the main tracking device of ALICE assuring up to 159[1] points in 3D-space for each track. The TPC also contributes to PID by meassuring the energy lost by particles while traveling trough it. This way the specific energy loss of particles can be determined and coupled to particle identities, as can be seen in figure 5. Trough the measured points, the TPC measures the momentum of charged particles, and is cabapable of identifying decay-vertices present in the data-sample. The pseudo-rapidity coverage of the TPC in the used ALICE datasets is also $|\eta| < 0.9$. Lastly, the TPC has a p_t-coverage of about $0.2 < p_t < 100$ GeV/c[7].

2.3.3 Time Of Flight detector (TOF)

The TOF is mainly there for particle identification. With this subdetector, ALICE can distinguish between protons, kaons and pions in the intermediate momentum range, which means $p < 2.5$ GeV/c for pions and kaons and $p < 4$ GeV/c for protons. The TOF distinguishes between particles trough their time-of-flight difference. It registrates momentum and velocity, and can distinguish particles by the seperation of these tracks caused by their difference in mass, as can be seen in figure 7. The TOF has pseudorapidity coverage $|\eta| < 0.9$. The presicion of p/K and K/π seperation of the TOF is better than 3σ.[7] The basic unit out of which the TOF detector consists is a 10-gap double-stack MRPC strip, of which a schematic view can be seen in figure 6.

2.3.4 High Momentum Particle Identification Detector (HMPID)

The main objective of the HMPID is to enhance particle identification for particles with momentum higher than 1 GeV/c. Particles with lower momentum can be identified by the ITS and TOF. Particle identification for particles traveling at higher momentum can be improved by the HMPID[7].

[1]Sum of inner and outer readout chamber pad rows.[7]

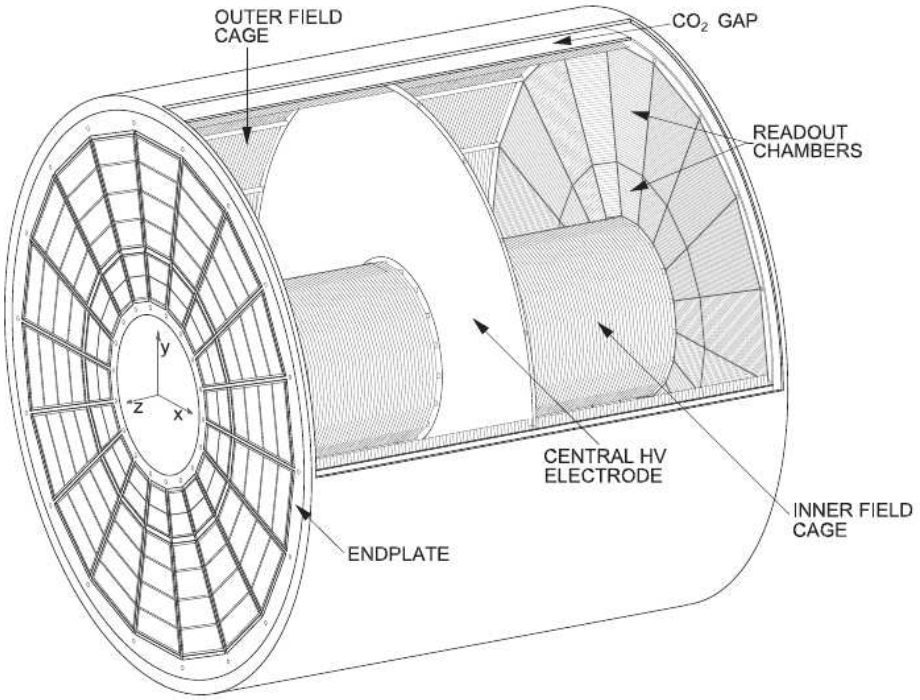

Figure 4: Schematic View of the ALICE TPC.[9]

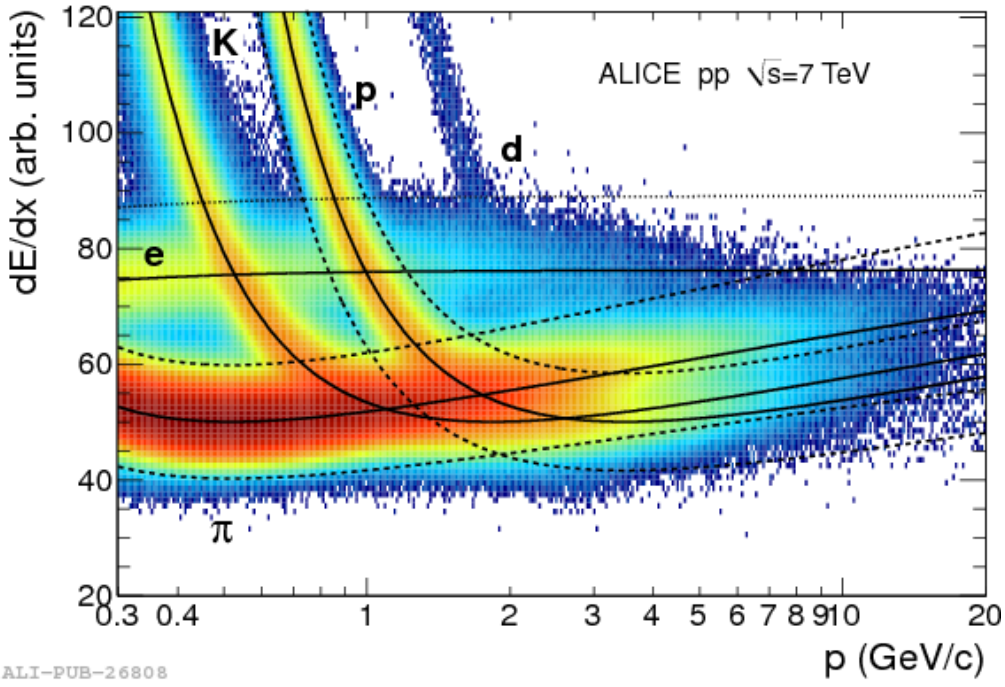

Figure 5: PID in TPC trough specific energy loss in pp collisions at $\sqrt{s} = 7$ TeV.[10]

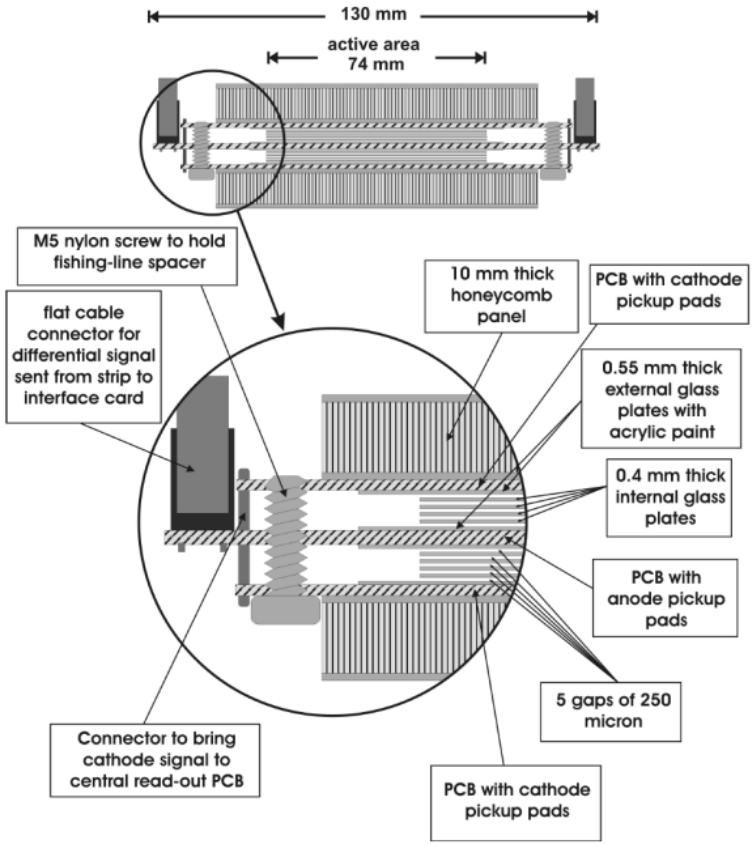

Figure 6: Schematic view of an MRPC strip.[7]

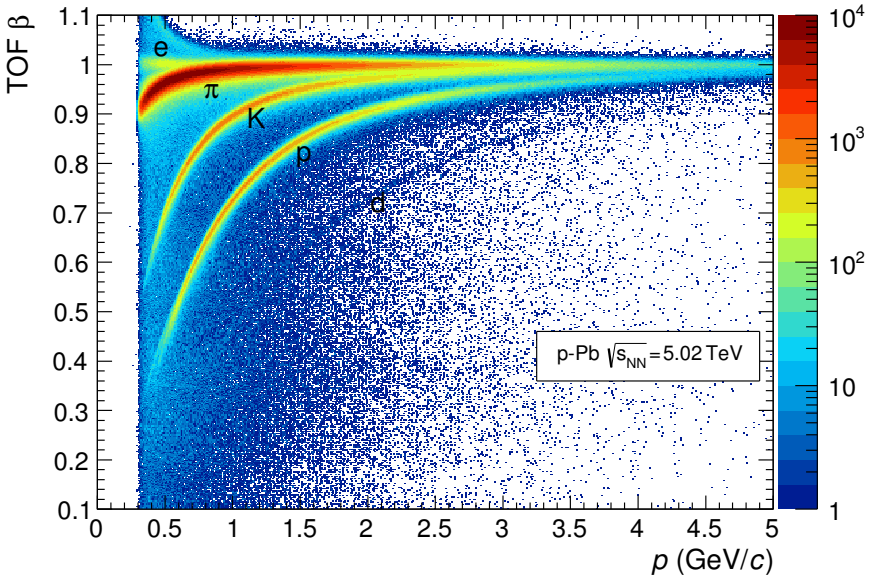

Figure 7: PID in TOF trough mass difference in p-Pb collisions at $\sqrt{s} = 5.02$ TeV ($\beta \equiv v/c$).[11]

2.4 Particle information

An understanding of certain properties of the particles reviewed in this thesis is nescesary. Certain properties of Σ_c, Λ_c and pions are used for the reconstruction of the Σ_c and will be discussed below.

2.4.1 The Σ_c-baryon

In this thesis, whenever the Σ_c-baryon is mentioned, a refference is made to both the Σ_c^{++}-baryon, the Σ_c^0-baryon and their anti-particles. According to theory, both the mass and the lifetime of these baryons differs only slightly, and both particles have only one decay channel according to which they decay. These decay channels are given by

$$\begin{aligned} \Sigma_c^{++} &\rightarrow \Lambda_c^+ \ \pi^+ \ (100\%) \\ \Sigma_c^0 &\rightarrow \Lambda_c^+ \ \pi^- \ (100\%)[4]. \end{aligned} \tag{9}$$

The prediction that the offset of the baryon-to-meson-ratio Λ_c/D^0 stems from Σ_c being created at the primary vertex during pp and p-Pb collisions is a reasonable one. Because the mean distance traveled by the Σ_c is $c\tau \approx 1 * 10^{-13}$ m [2]. As seen in figure 2, the ALICE measuring apparatus is able to determine the location of the primary vertex with a precision of less than 100 μm. The distance traveled by a Σ_c is significantly smaller, resulting in the particle decaying into a pion and a Λ_c before it has traveled outside of ALICE primary vertex precision range. Because of this, it is impossible to determine wether a Λ_c is a prompt particle or the decay product of a Σ_c-baryon.

The Σ_c-baryon can have different masses due to the fact that the particle can be in different quantum states i.e. have different resonances. The expected invariant masses for two of those resonances are stated below:

$$\begin{aligned} m(\Sigma_c^{++}[2455]) &= 2453.97 \pm 0.14 \ \mathrm{MeV/c^2} \\ m(\Sigma_c^{++}[2520]) &= 2518.41^{+0.21}_{-0.19} \ \mathrm{MeV/c^2} \\ m(\Sigma_c^{0}[2455]) &= 2453.75 \pm 0.14 \ \mathrm{MeV/c^2} \\ m(\Sigma_c^{0}[2520]) &= 2518.48 \pm 0.20 \ \mathrm{MeV/c^2}[4] \end{aligned} \tag{10}$$

[2] The width Γ of the Σ_c was obtained from the pdg-database and converted into mean lifetime according to $\tau = \frac{\hbar}{\Gamma}$[4]

2.4.2 The Λ_c-baryon

The decay channel used for the reconstruction of the Λ_c from the data runs is the channel

$$\Lambda_c^+ \rightarrow \mathrm{p}\ \mathrm{K}^-\ \pi^+\ (6.35 \pm 0.33\%)[4] \tag{11}$$

Note that the fact that only this channel is used means that a maximum of 6.35% of all Λ_c-candidates can be reconstructed[3]. The mean distance traveled by the Λ_c before decay is $c\tau \approx 6 * 10^{-5}$ m[4]. This distance is also too short to travel outside of the primary vertex precision range of ALICE. This means all Λ_c must be reconstructed from properties of the daughter particles detected in the ALICE aparatus. An invariant mass analysis must be applied.

2.4.3 Pions ($\pi^{\pm}$)

In this thesis, whenever pions (π) are mentioned, a refference is made to π^+ and π^-, but not to π^0. Pions are the most common type of meson, resulting in the fact that there is an enormous amount of pions being created with each pp collision. The mean distance traveled by a pion is given by $c\tau \approx 8$ m[4]. This means that pions which travel within the pseudo-rapidity coverage of the ALICE detector can very well be detected by the experimental apparatus. The majority of particles produced in the collisions are pions. Therefore, there is a large combinatorial background once an attempt is made to add a pion track to a Λ_c-candidate in order to form a Σ_c-candidate. To attempt to largely reduce the combinatorial background, it is useful to study the properties of pions coming from true Σ_c decays. These properties could differ from those of the sample of all inclusive pions created in the collisions. The transverse momentum of the pions will be the specific property that is researched. In case differences are found, they can be of aid in setting selection criteria to reject Σ_c-candidates coming from pure combinatorial background.

3 Analysis

3.1 Simulations

To simulate a variety of expected p_t-distributions for pions, Pythia8 version 8186[12] was used. Pythia8 was connected to ROOT[13] in order to be able to write in ROOT syntax[4] rather than Pythia8 syntax. The version of ROOT that was used is ROOT6.14.04[14]. A pre-made macro titled 'pythia8.C' was adopted. This macro can be found among the tutorials on the ROOT webpage[15]. The macro was adapted to simulate the desired event and to select only those particles and properties which are useful to this research. The simulations were forced such that with each pp collision simulated, at least one charm/anti-charm quark

[3]Not all Λ_c are the decay product of Σ_c, so the chances of actually achieving a reconstruction of 6.35% are practically zero.

[4]ROOT is a C++ based program.

pair was formed. In reality, charm/anti-charm quark pairs are formed considerably less often. This forcing allowed for the acquisition of significant results in less time than it would have taken without the forcing. While this forcing was active, the kinematics of the decay were set to match realistic ones. In the appendix, the full code used in the macro is shown. The following lines of code from the macro allow for the charm forcing mentioned above when using Pythia8 combined with ROOT:

```
pythia8->ReadString("HardQCD:all = on");
pythia8->ReadString("HardQCD:gg2ccbar = on");
pythia8->ReadString("HardQCD:qqbar2ccbar = on");
pythia8->ReadString("phaseSpace:pTHatMin = 50.");
```

Particle selection was restricted to particles within pseudorapidity range $|\eta| < 0.9$ to match with that of the ALICE data. The collision energy was set at $\sqrt{s} = 5$ TeV. Of each selected particle, the transverse momentum (p_t) was requested, and subsequently put in a histogram. A selection of particles with specific mother-particles was also made, meaning those particles are the decay product of a specific particle. All pions which had Σ_c as mother particle were selected, from hereon out called 'soft pions'. Moreover, all soft pions arising from the pp collisions were selected, with the extra criterion that the p_t of the Σ_c (before decay) lies within a certain range. These last histograms were created, because a difference in the p_t-distribution of all pions from Σ_c and pions from Σ_c in different Σ_c p_t-bins is likely to be observed. All histograms are divided by their total number of entries in order to normalize them to 1. An overview of the histograms generated and used for analysis can be seen in table 2.

Table 2: Histograms generated for analysis

Histogram	**Particles**	**mother particle**	**mother particle p_t(GeV/c)**
All Pions	π	N/A	N/A
All soft pions	π	Σ_c	N/A
Soft pions 1	π	Σ_c	[1,2]
Soft pions 2	π	Σ_c	[2,3]
Soft pions 3	π	Σ_c	[3,4]
Soft pions 4	π	Σ_c	[4,6]
Soft pions 5	π	Σ_c	[6,12]
Soft pions 6	π	Σ_c	[12,→⟩

Note that in the histograms in table 2, no distinction was made between the two kinds of pions and their different Σ_c mother particles. This distinction was left out, because it is reasonable to expect that the p_t-distributions of a particles of the same mass ($\pi^{\pm}$), with mother particles which have equal mass or approximately equal mass $((\Sigma_c^{++}, \Sigma_c^{--})$, $(\Sigma_c^0$, $\bar{\Sigma}_c^0))$, will be within the same range. By taking into account all pions which can possibly be reconstructed into Σ_c, the amount of entries in the histograms is maximized, which results in the best resolution. The p_t-distributions of the simulated soft pions (signal) can be compared to that of all inclusive pions (background). Dividing the signal pion p_t-distributions by the background pion p_t-distribution results in signal v.s. background ratio plots. From these plots the p_t-value at which the signal surpasses the background can be obtained. At these p_t-values, the data from the ALICE runs should be cut to decrease the amount of background pions.

To be able to get an insight on the p_t-range in which soft pions coming from Σ_c with a certain p_t lie, we filled a histogram with Σ_c p_t v.s. soft pion p_t.

3.2 Comparison with ALICE data

The pions from the ALICE datasets undergo a specific selection process. Firstly, the invariant mass of Λ_c was reconstructed trough a data analysis which is outside the scope of this thesis. Around the reconstructed Λ_c invariant mass signal, a region of 3σ was cut out. The reconstructed Λ_c invariant mass was combined with pions from the ALICE dataset.[5] Next the invariant mass of the Λ_c was subtracted from the $\Lambda_c + \pi$ invariant mass. A 10 MeV region was cut out around the expected invariant mass difference $m(\Lambda_c\, \pi) - m(\Lambda_c)$. Only the p_t of pions which were used for the reconstruction of Σ_c-candidates that are in this specific region was selected. To the pion p_t-distributions that remain, the cuts originating from the simulations can be applied. Firstly, in the ALICE data only pions in a p_t-range of $p_t \in [0.02, 24.00]$ GeV/c were analyzed. Secondly, only Σ_c^{++} were subjected to reconstruction. The Σ_c^{++} p_t-bins that where used in the ALICE data are $p_t \in \{[2,3],[3,4],[4,6],[6,8],[8,12],[12,24]\}$ GeV/c. So to compare this data to the Pythia8 simulations, the histograms with Σ_c $p_t \in [6,8]$ GeV/c and Σ_c $p_t \in [8,12]$ GeV/c had to be merged. All histrograms obtained from the ALICE data were normalized to 1 by dividing them through their total amount of entries.

The pion p_t histograms from the ALICE data were compared to the ones that arised from simulations in Pythia8. For each Σ_c p_t-bin, the ALICE data p_t-distribution was plotted on top of the simulated one. From these comparison plots, an indication of the amount of similarity between the Pythia8 simulations and the actual data acquired by the ALICE detector was obtained.

[5] An important note is that not only the invariant mass of the pion contributes to the invariant mass of the Σ_c-candidate. Each pion has a kinetic energy which also contributes to the invariant mass of the Σ_c-candidate.

3.3 Fits to invariant mass distribution from ALICE data

After the cuts found in the analysis with Pythia8 from section 3.1 were applied, the reconstruction of Σ_c was attempted. As described before, Λ_c^+-candidates from the ALICE data-sets were combined with π^+ tracks, and reconstructed into Σ_c^{++}-candidates. The invariant mass of these candidates was determined using equation 3. In each Σ_c p_t-bin, the invariant mass of the Σ_c^{++}-candidates was taken. Next the invariant mass of the Λ_c^+-candidates was subtracted from the Σ_c^{++} invariant masses. The histograms originating from the previous steps were fitted. The fitting function used consists of a second order polynomial as the background function and a Gaussian as the signal function. If a signal peak can be observed in one of the Σ_c p_t-bins at the expected invariant mass difference

$$m(\Lambda_c^+ \, \pi^+) - m(\Lambda_c^+) = 167.510 \pm 0.022 \text{ GeV/c}^2, [4] \tag{12}$$

this would hint at the possibility of reconstruction of the Σ_c from ALICE data. If a peak with a significance of $\alpha > 3$, and a width of about 6 MeV/c^2 can be observed, this will classify as an observation of the Σ_c^{++}. Using data acquired by the ALICE detector to reconstruct Σ_c will then be proven to be achievable. Further research into the offset of the baryon-to-meson ratio Λ_c/D^0 trough reconstruction of the Σ_c would then be promising.

The invariant mass difference histograms with h Σ_c $p_t \in [6, 8]$ GeV/c and Σ_c $p_t \in [8, 12]$ GeV/c were available from the ALICE data. Although these Σ_c p_t-bins where not simulated in Pythia8, fits to these histograms where processed into this thesis.

4 Results

4.1 Simulations

The normalized pion p_t-distributions acquired trough the simulation of 10 M charm-forced pp collisions at $\sqrt{s} = 5$ TeV can be seen in figure 8 below. Comparing the p_t-distribution of inclusive pions with that of soft pions from the Σ_c, it can be seen there's a difference between the two distributions. The p_t-distribution of inclusive pions will from hereon be called 'the background'. The peak of the soft pion distribution is shifted to the left of the p_t-distribution of the background. This shift has an effect on the mean of the distribution. The mean shifts from a value of $p_t = 0.614$ GeV/c for the background to a value of $p_t = 0.606$ GeV/c for soft pions.

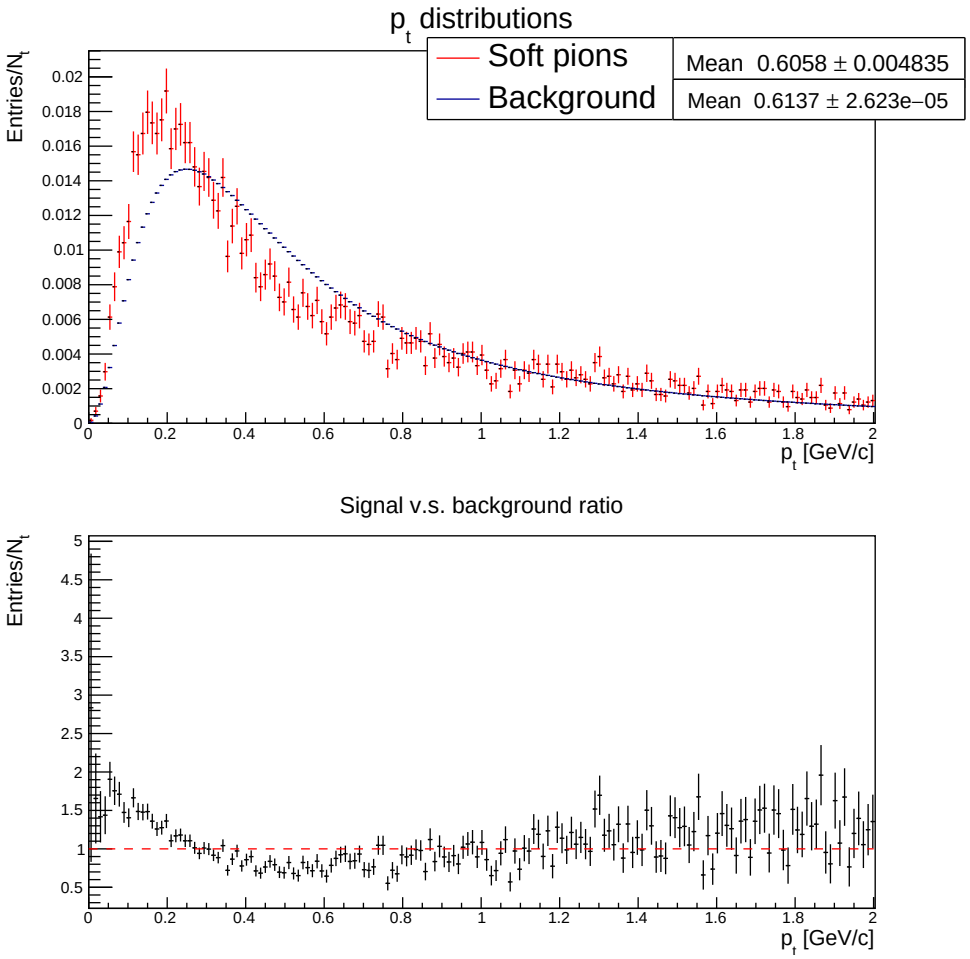

Figure 8: Comparison between simulated p_t-distribution of background pions and that of simulated soft pions from Σ_c. In the ratio plot, the dashed red line indicates where the soft pion signal surpasses the background.

The observed differences are useful as an indication that the p_t-distribution of soft pions differs from that of the background pions. However, looking at the ratio plot in figure 8, it can be observed that the p_t-distribution of soft pions at full p_t-range of the Σ_c is not useful for finding cutting values to the ALICE data. In the range $p_t \in [0, 0.3]$ GeV/c, the signal is higher than the background. In the range $p_t \in [0.3, 0.7]$ GeV/c the background overtakes the signal, and starting at $p_t \approx 0.7$ GeV/c The ratio plot keeps fluctuating around a value of 1.

In the results below, comparisons between the p_t-distribution of background pions with that of soft pions from Σ_c in different Σ_c p_t-bins can be seen. The p_t-bins used for the Σ_c are $p_t \in$ {[1,2] , [2,3] , [3,4] , [4,6] , [6,12] , [12,→⟩} GeV/c.

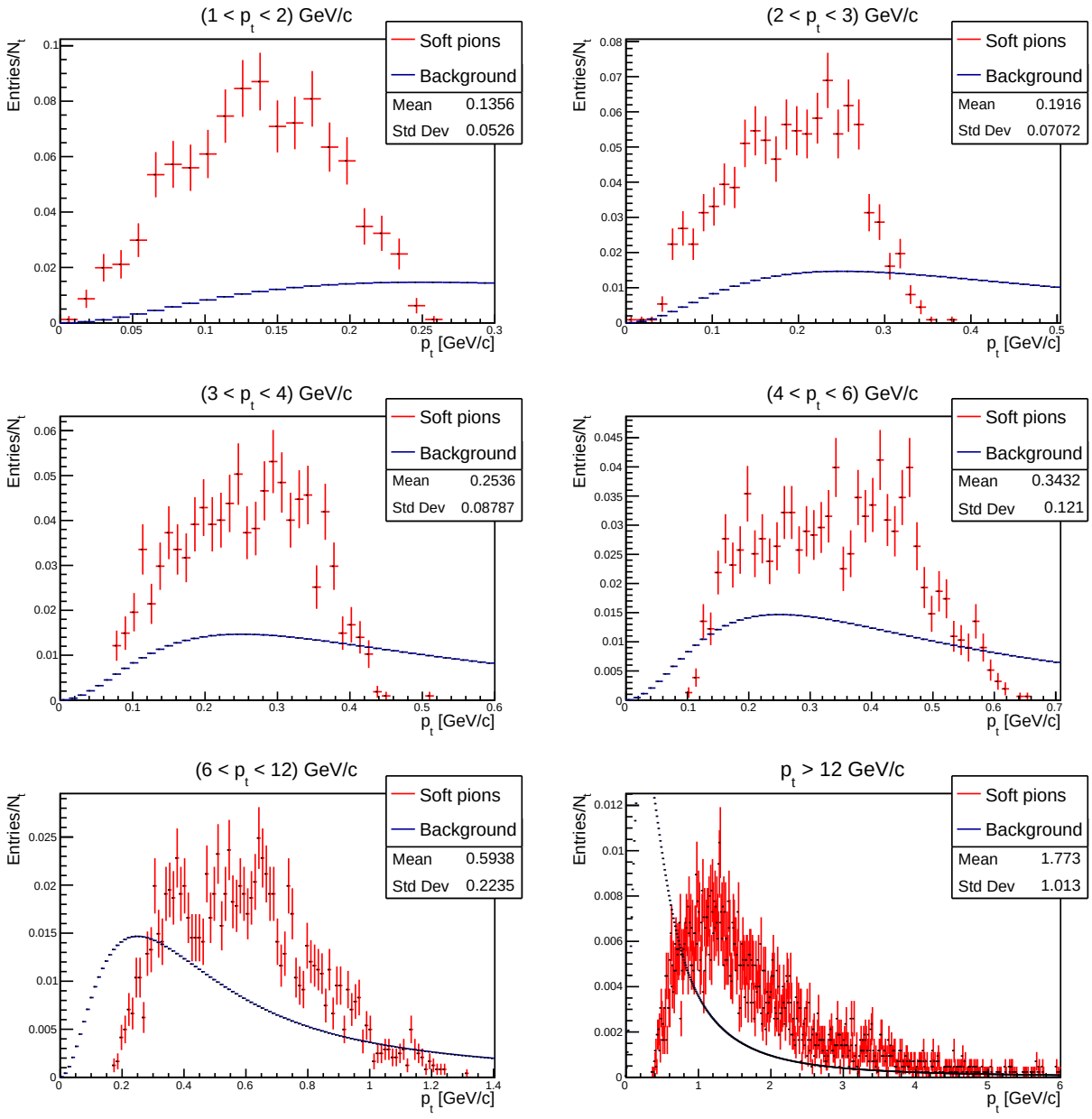

Figure 9: Comparison between p_t-distributions of simulated soft pions from Σ_c and simulated background pions in different Σ_c p_t-bins. The range of the figures has been adapted to fit the p_t-values of the simulations. N_t is the total amount of entries. The stats displayed are those of the soft pion p_t-distribution

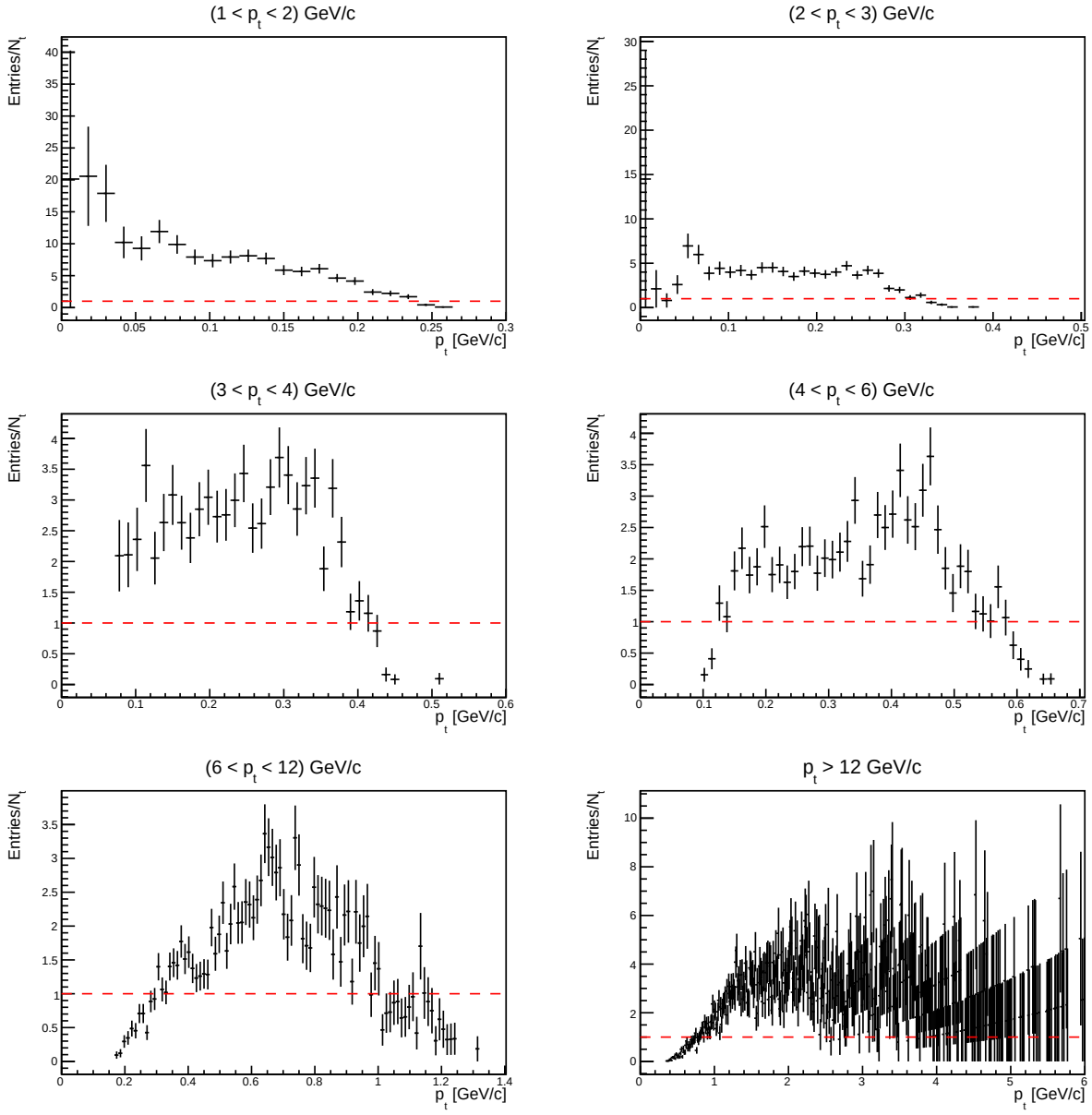

Figure 10: Ratio plots of simulated soft pions and simulated background pions p_t-distributions in different Σ_c p_t-bins. The dashed red line indicates where the signal becomes larger than the background. N_t is the total amount of entries.

Using the ratio plots from figure 10, the bins at which cuts could be made were extracted. Since the histograms in figure 9 and 10 have the same total amount of bins, the first cut for each Σ_c p_t-bin could be made at the first bin at which the ratio plot exceeds a value of 1 (X1). The second cut for each Σ_c p_t-bin could be made at the last bin at which the ratio plot exceeds a value of 1 (X2). The histogram for each Σ_c p_t-bin was integrated from X1 to X2. The value obtained gives a prediction on how much of the signal from the ALICE data remains after the cuts have been applied. For each Σ_c p_t-bin, an integral over the background pion p_t-distribution was taken. This integral was also taken from X1 to X2. This way the predicted effect of the cuts on the background was obtained.

Table 3: Expected effect of cuts on signal and background

p_t bin (GeV/c)	**Cuts made at (GeV/c)**	**Background removed (%)**	**Signal lost (%)**
[1,2]	0.006 - 0.234	82.7	0.7
[2,3]	0.006 - 0.318	72.6	1.4
[3,4]	0.078 - 0.414	63.3	1.4
[4,6]	0.126 - 0.582	52.3	1.7
[6,12]	0.306 - 1.146	49.5	9.0
[12,→⟩	0.750 - 9.59	62.3	9.7

Observing figure 9, the peak of the soft pion p_t-distribution can be seen to shift to the right as higher Σ_c p_t-bins are analysed. The mean of the soft pion p_t-distributions is seen to be increasing with each Σ_c p_t-bin as a confirmation. With each higher Σ_c p_t-bin, the difference between signal and background seems to becomes more significant. In Table 3, it can be seen that the expected effect of the cuts on the background declines while moving to higher Σ_c p_t-bins. In the last bin the expected effect on the background goes up again. The expected effect of the cuts on the signal increases while moving to higher Σ_c p_t-bins.

To give a clear indication of the p_t-range in which the p_t of daughter pions of Σ_c lies, the results of Σ_c p_t v.s. daughter pion p_t from the simulations can be seen in figure 11.

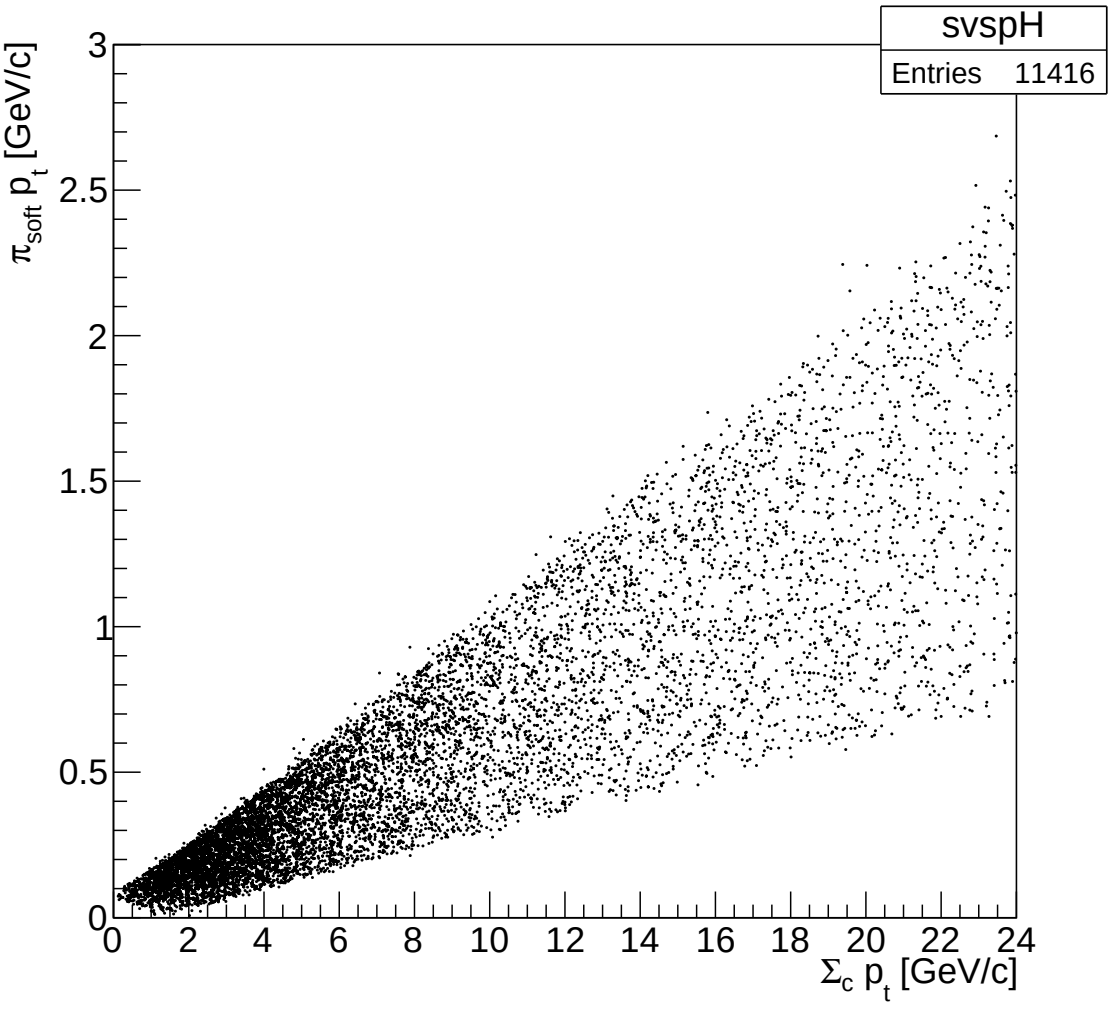

Figure 11: Σ_c p_t v.s. soft pion p_t. Note that on average, for higher Σ_c p_t, the amount of entries declines. Also, the pion p_t data points spread out for higher p_t-values of Σ_c.

Table 4: Σ_c p_t-range with daughter pion p_t-range observed in figure 11

$\mathbf{\Sigma_c\ p_t}$ **range (GeV/c)**	**Daughter pion** $\mathbf{p_t}$ **range (GeV/c)**
[1,2]	[0.01 , 0.26]
[2,3]	[0.01 , 0.38]
[3,4]	[0.07 , 0.51]
[4,6]	[0.10 , 0.65]
[6,12]	[0.17 , 1.31]
[12 , 24]	[0.36 , 2.69]

4.2 Comparison with ALICE data

Comparing the soft pion p_t-distributions simulated by Pythia8 with the selected pion p_t-distributions from ALICE data described in section 3.2, the results shown in figure 12 were found.

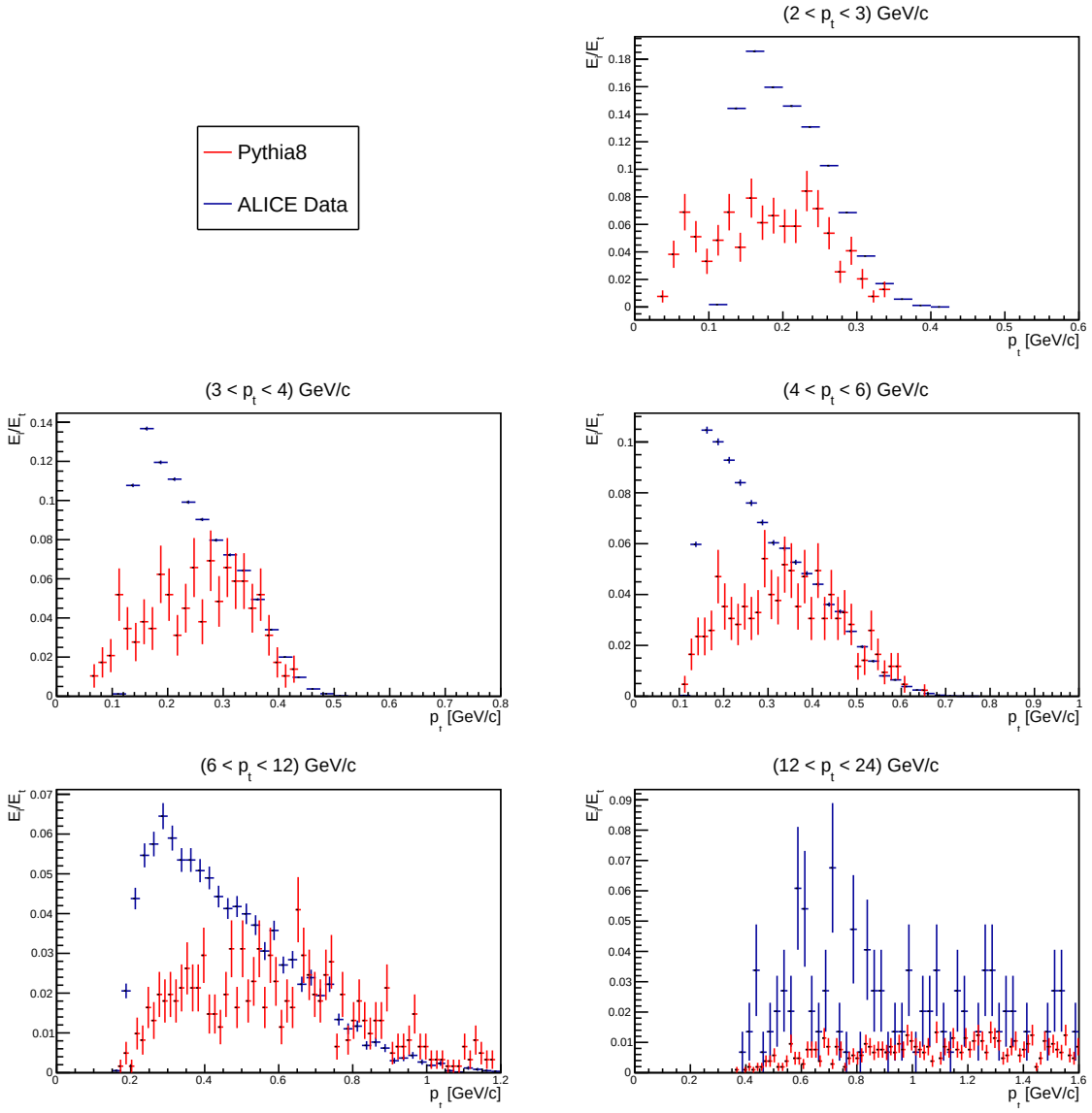

Figure 12: Comparison of Pythia8 soft pion p_t-distributions in different Σ_c p_t-bins and selected pion p_t-distributions from ALICE data.

The Σ_c p_t-bin [1,2] GeV/c was left out. The reason for this, is that pions decaying from Σ_c with low p_t-values like this, have such low-valued p_t-distributions that selection from the ALICE data was impracticable. This is the case, because the ALICE detector has difficulty detecting particles that have $p_t < 100$ MeV/c.

4.3 Fits to invariant mass distribution from ALICE data

The invariant mass analysis from section 3.3 was applied around the expected invariant mass of $\Sigma_c^{++}[2455]$. Trough this analysis, it should be uncovered whether a Σ_c signal can be observed at the position of the expected invariant mass difference. As stated before, because the pion p_t histograms of Σ_c p_t-bins [6,8] GeV/c and [8,12] GeV/c were available from the ALICE data, fits were also attempted to these histograms. It has to be noted that there were problems in the implementation of the selection criteria below 6 GeV/c.

Taking a look at figures 13 and 14, it is clear that the fits return better results in some p_t-bins than in others. Note that along the data points of Σ_c p_t-bin [3,4] GeV/c, although the signal peak trough this data point is of very low significance, a small fluctuation can be seen around the location of the Gaussian signal peaks from the fits to Σ_c p_t [4,6] GeV/c, [6,12] GeV/c and [6,8] GeV/c.

The fit to Σ_c p_t [12,24] GeV/c shows a dip around the expected invariant mass difference. The fit to the datapoints in Σ_c p_t-bin [8,12] GeV/c shows a peak at the expected invariant mass difference. It was therefore decided to merge these histograms and see what a fit to the new histogram with Σ_c $p_t \in [8, 24]$ GeV/c returns. The result can be seen in figure 15.

The invariant mass analysis from 3.3 was also attempted around the expected invariant mass difference of $\Sigma_c^{++}[2520]$. Unfortunately, no successful fits to the ALICE data could be made in this region.

The mean of the signal functions which showed a Gaussian peak was compared with the expected invariant mass difference. It was decided to leave out the signal peaks from the histograms with Σ_c $p_t \in \{[2, 3], [3, 4], [6, 12]\}$. In the case of the first two due to low significance of the peaks. In the case of the last due to the fact that the fit does not follow a signal peak which is observable in the ALICE data. The marker is set in the middle of each p_t-bin and the horizontal error-bar spans the width of each bin. The vertical error is the standard deviation extracted from the signal functions of the fits. This comparison can be seen in figure 16. The standard deviation of each of the obtained invariant mass differences can be seen in figure 17.

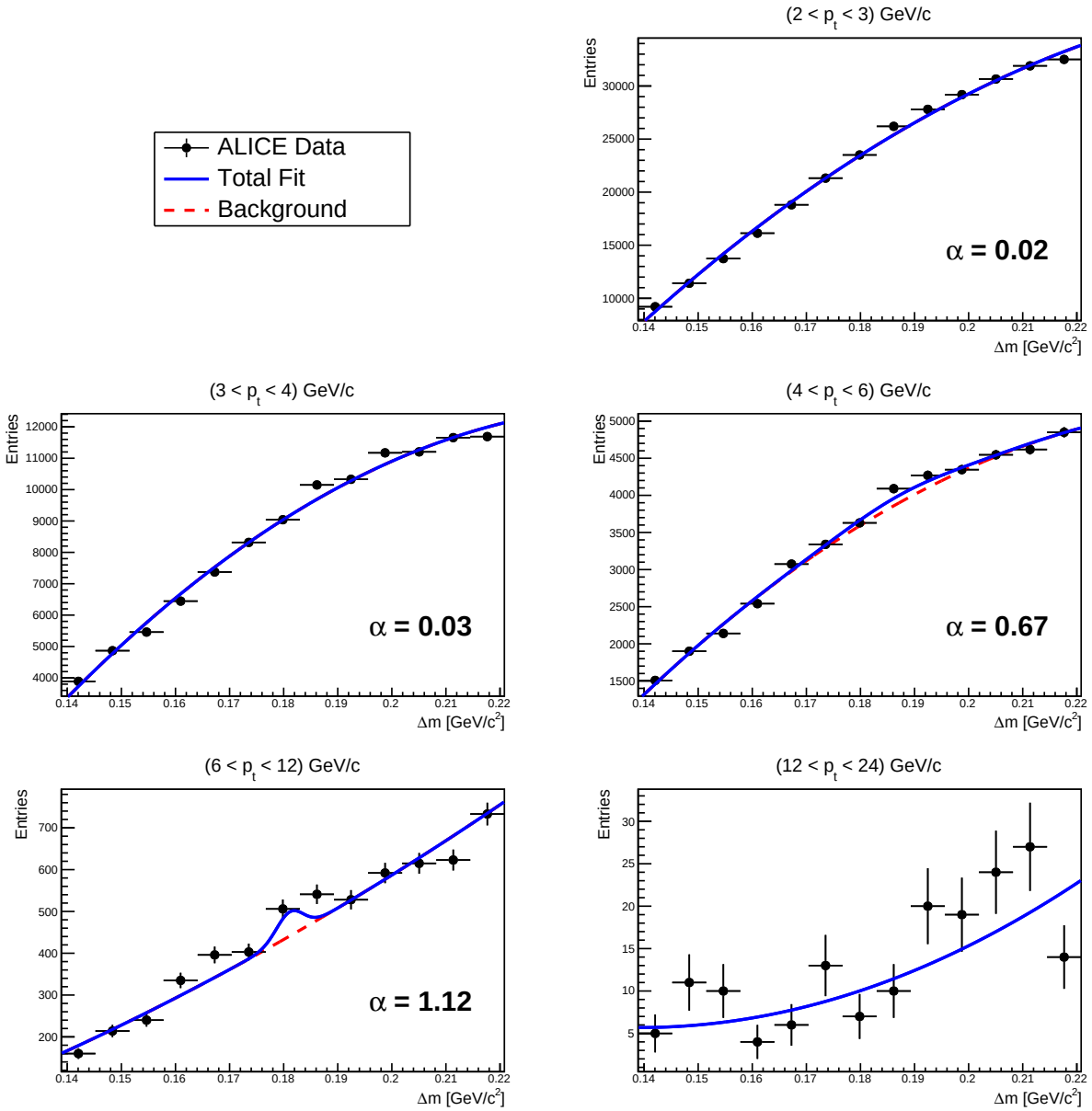

Figure 13: Fits to the invariant mass difference $m(\Lambda_c^+ \pi^+) - m(\Lambda_c^+)$ for the different histograms extracted from ALICE data. Significance (α) added where relevant.

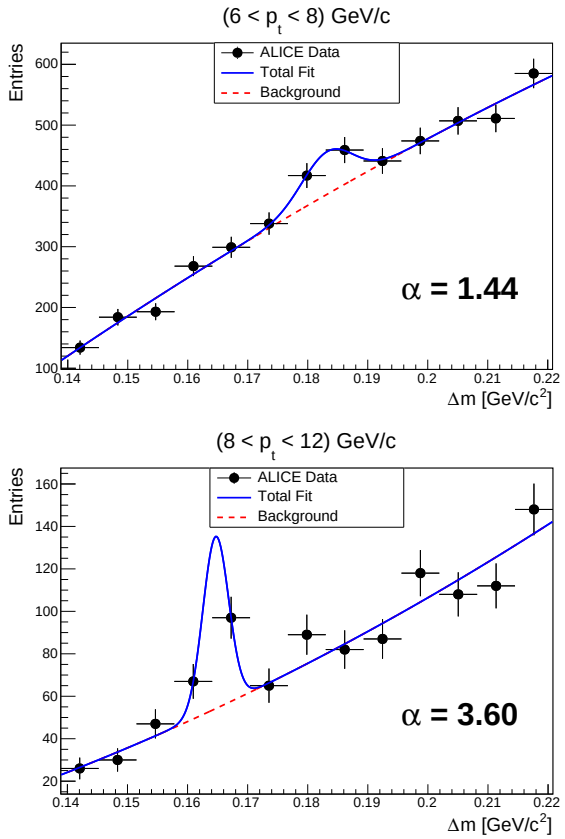

Figure 14: Fit to the invariant mass difference $m(\Lambda_c^+ \ \pi^+) - m(\Lambda_c^+)$ for histograms from ALICE data with Σ_c $p_t \in [6, 8]$ and $[8, 12]$ GeV/c.

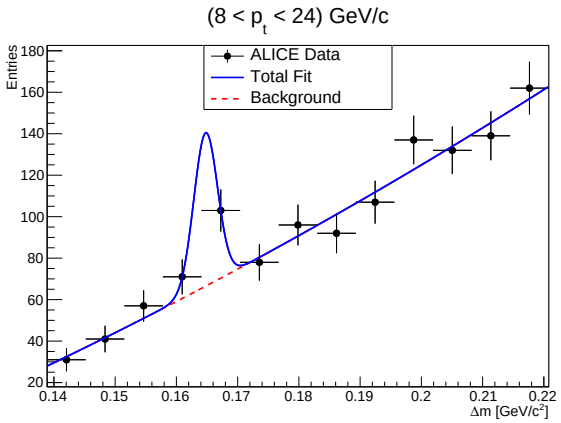

Figure 15: Fit to the invariant mass difference $m(\Lambda_c^+ \ \pi^+) - m(\Lambda_c^+)$ for histograms from ALICE data with Σ_c $p_t \in [8, 12]$ GeV/c and Σ_c $p_t \in [12, 24]$ GeV/c combined.

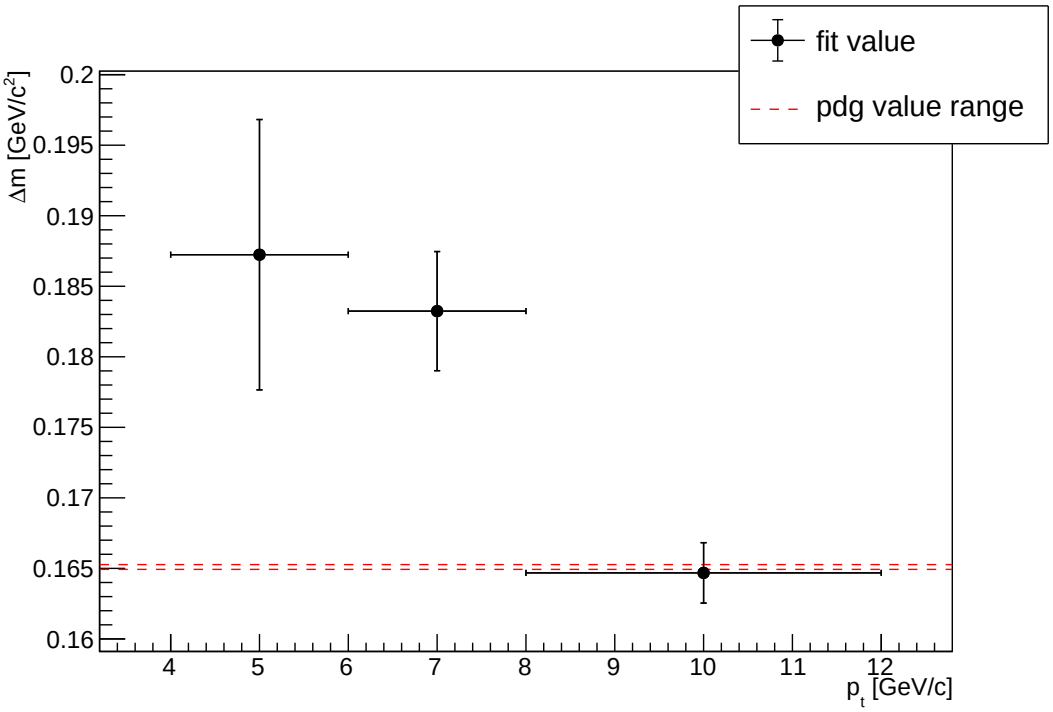

Figure 16: Comparison of the reconstructed signal with the expected position[4] of the signal for Σ_c p_t-bins with $p_t \in \{[2,3],[3,4],[4,6]\}$GeV/c.

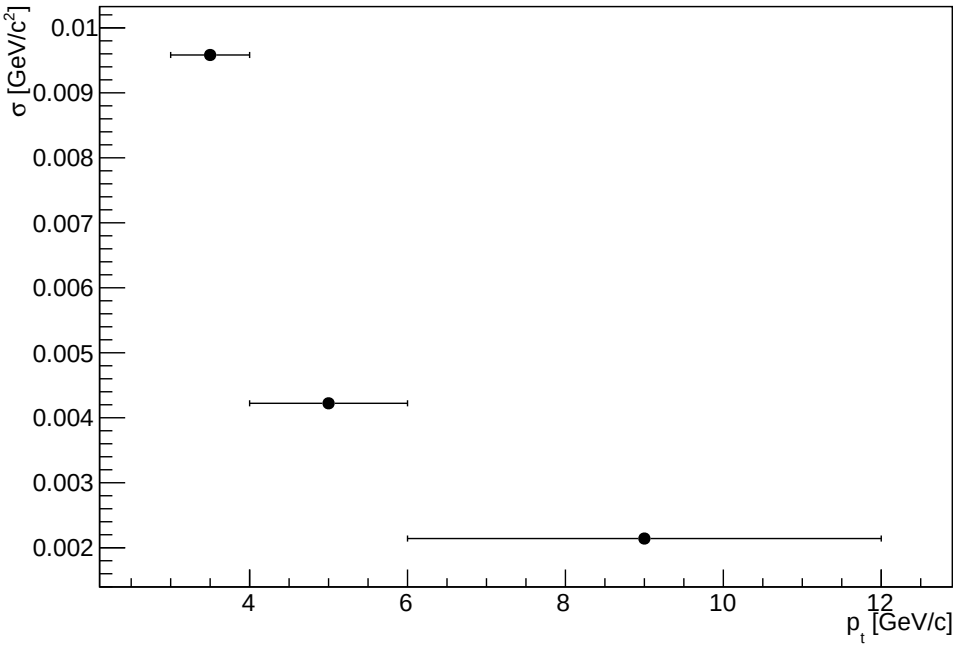

Figure 17: Gaussian peak width of the reconstructed signal from figure 16.

5 Conclusions

From figures 9 and 10, and from table 3, it was pointed out that the simulations in Pythia8 (version 8.168) were able to provide useful information. Cutting values to apply to the pion p_t-distribution used for Σ_c-reconstruction from the ALICE data were succesfuly found. Comparison of the simulated p_t-distributions of soft pions with that of simulated inclusive pions predicted the effect the cuts would have on each Σ_c p_t-bin.

Observing figure 12, an indication of the overlap between the Pythia8 simulations and the ALICE data was given. The p_t-distributions mainly show overlap around the end of each histogram. The p_t-values at which the pion p_t-distributions begin, overlap for the last three Σ_c p_t-bins. The p_t-values at which the pion p_t-distributions end, overlap for Σ_c p_t-bins with $p_t \in \{[3,4],[4,6],[6,12]\}$. All histograms show that the amount of pions counted around the beginning of the pion p_t-distribution is much higher in the ALICE data than in the simulated p_t-distributions of soft pions from Σ_c. This requires further discussion.

Looking at figure 13 and 14, hints of peaks can be observed in the bins with Σ_c $p_t \in [6,8]$ GeV/c and Σ_c $p_t \in [8,12]$ GeV/c. The fact that no clear peak can be observed in the bin with $p_t \in [12,24]$ GeV/c, can be attributed to the large statistical error present within the ALICE data in this bin. The dip which is present around the expected position of the signal peak in the bin with $p_t \in [12,24]$ GeV/c was proven to be a statistical fluctuation. Observing figure 15, it can be seen that the dip completely disappears in the histogram with Σ_c $p_t \in [8,24]$ GeV/c.

From figure 16 it can be recognized that the peak in the bin with $p_t \in [8,12]$ GeV/c provides a signal at the expected location. This peak has a significance of $\alpha = 3.60$, which would mean it can be classified as an observation of the Σ_c^{++}. However, because the fit trough the signal peak only goes trough 2 data-points and its standard deviation lies below the expectation value, it will only be classified as 'a hint of a peak'. The deviation from the expected location that the signals in the Σ_c p_t-bins with $p_t \in [4,6]$ GeV/c and $p_t \in [6,12]$ GeV/c show, requires further discussion.

As stated before, there were problems in the implementation of the selection criteria (cuts) below 6 GeV/c. A fix to these problems was already found, and the new data analysis is running at the time this thesis is written. Final results will be available in a week. However unfortunate, evidence of the strength of the kinematical cuts on the soft pion p_t spectra *were* found in this thesis. In fact, in the p_t-regions where they were applied without problems ([6,8] and [8,12] GeV/c) a hint of a Σ_c-signal appears.

Observing the results found in this thesis, the reconstruction of the Σ_c-baryon with the ALICE detector at CERN seems feasible. With further research, discoveries concerning the production rate of Σ_c at the primary vertex in pp and p-Pb collisions with center of mass energies in the TeV energy-scale could be made. With such discoveries, adaptations to the baryon-to-meson (Λ_c/D^0) ratio found in the ALICE paper[1] could be made.

6 Discussion and further prospects

6.1 Discussion

Taking a look at the simulation v.s. ALICE data comparison shown in figure 12, it can be seen that the ALICE data differs from the simulations. The amount of pion entries in the ALICE data is considerably higher at the beginning of the p_t-distribution in each Σ_c p_t-bin. This could be caused by the fact that pions coming from different decays could enter the pion selection from the ALICE data. If a pion comes from a different decay, but has a p_t-value which is comparable to the p_t of the ones used for Σ_c-reconstruction, it could be selected. This is an effect of the large combinatorial background formed by the pions.

In figure 13 and 14, a peak which is shifted from the expectation value appears in the bins with Σ_c $p_t \in ([4,6],[6,8])$ GeV/c and a small fluctuation can be seen around the same position in the Σ_c $p_t \in [1,2]$ GeV/c bin. This shift could be caused by misalignment of the ALICE sub-detectors. Misalignment of the detectors causes a greater shift in x- and y-coördinates for lower-p_t particles than it does for high-p_t particles. A shift in coördinates could cause a decrease in p_t measured for these particles. Using equation 3, this would result in an increase in the invariant mass calculated for these low-p_t particles, explaining the shift of the invariant mass to a higher value than expected.

6.2 Outlook

As pointed out before, further research into the Σ_c-baryon could be promising in the road to finding the cause of the offset in the Λ_c/D^0-ratio.

Future research could include reconstruction of the invariant mass of the remaining Σ_c (Σ_c^{--}, Σ_c^0, $\bar{\Sigma}_c^0$). With these reconstructions, it would be possible to determine whether the expectation that pions coming from any of the Σ_c will have a similar p_t-distribution is justified. Since Σ_c^{--} is Σ_c^{++}'s anti-particle, and pions coming from this particle have the same p_t-distribution by definition, it would be most interesting to reconstruct one of the Σ_c^0-baryons.

Another option for further research would be to apply changes to the cuts used for Λ_c^+-reconstruction mentioned in section 3.2. The cuts that were applied in favour of the reconstruction of Λ_c^+ optimized that specific reconstruction, but probably do not have optimal effect on the reconstruction of Σ_c^{++}. By loosening the cuts made for Λ_c-reconstruction, and thus sacrificing the optimal reconstruction cuts for Λ_c^+, the reconstruction of Σ_c^{++} could possibly be improved.

Moreover, it would be interesting to see what could be found in the ALICE datasets which will be generated when the upgrades planned for ALICE have been installed after the second long shutdown (LS2, 2018-2019). The tracking precision of the ALICE detector will have increased[16] and using the newly generated datasets for similar research will most likely pay off.

References

[1] ALICE collaboration. *Λ_c^+ production in pp collisions at $\sqrt{s} = 7$ TeV and in p-Pb collisions at $\sqrt{s_{NN}} = 5.02$ TeV*. 2017.

[2] Brian R. Martin. *Nuclear and Particle physics: An Introduction*, pages (3–6, 8). Wiley, 2009.

[3] The Constituent Particles of the Standard Model. https://commons.wikimedia.org/wiki/Standard_Model#/media/File:Standard_Model_of_Elementary_Particles.svg. Accessed: 22-12-2018.

[4] C. Patrignani et al. (Partilce Data Group). *Chin. Phys. C, 40, 100001.* pages (560, 1637–1646), 2016.

[5] S. Gupta. *A Short Introduction to Heavy Ion Physics*. page (6), 2014.

[6] ALICE Website. http://alice.web.cern.ch/. Accessed: 16-01-2019.

[7] K. Aamodt et al. *The ALICE Experiment at the CERN LHC. JINST*, pages (18, 201, 54, 74, 83, 76), 2008.

[8] Layout of the ITS. http://alice-publications.web.cern.ch/sites/alice-publications.web.cern.ch/files/papers/3907/its-rf-2-26925.png. Accessed: 08-01-2019.

[9] Layout of the TPC. https://www.researchgate.net/figure/Schematic-drawing-of-the-ALICE-TPC-3_fig1_318560304. Accessed: 08-01-2019.

[10] Particle Identification by Energy Loss in the TPC. https://cds.cern.ch/record/2242545/files/PID_tpc.png. Accessed: 08-01-2019.

[11] Particle Identification by Change in Velocity in the TOF. http://alice-publications.web.cern.ch/sites/alice-publications.web.cern.ch/files/papers/716/TOF_Performance_pPb-8504.pdf. Accessed: 08-01-2019.

[12] Pythia8 Version 8186 Download Link. http://home.thep.lu.se/~torbjorn/pythiaaux/recent.html. Accessed: 11-01-2019.

[13] ROOT with Pythia6 and Pythia8. https://root-forum.cern.ch/t/root-with-pythia6-and-pythia8/19211. Accessed: 15-01-2019.

[14] ROOT Version 6.14.04 Download Link. https://root.cern.ch/content/release-61404. Accessed: 11-01-2019.

[15] ROOT Tutorials: Pythia Event Generator. https://root.cern.ch/root/html/tutorials/pythia/pythia8.C.html. Accessed: 28-12-2018.

[16] R. Tieulent. *ALICE Upgrades: Plans and Potentials*. page (1), 2015.

[17] The ALICE Experiment, ALICE's eyes. http://aliceinfo.cern.ch/Public/en/Chapter2/Chap2Experiment-en.html. Accessed: 27-12-2018.

A Appendix

A.1 Runlist of ALICE data used

(282343, 282342, 282341, 282340, 282314, 282313, 282312, 282309, 282307, 282306, 282305, 282304, 282303, 282302, 282247, 282230, 282229, 282227, 282224, 282206, 282189, 282147, 282146, 282127, 282126, 282125, 282123, 282122, 282120, 282119, 282118, 282099, 282098, 282078, 282051, 282050, 282031, 282030, 282025, 282021, 282016, 282008).

A.2 The ALICE Detector

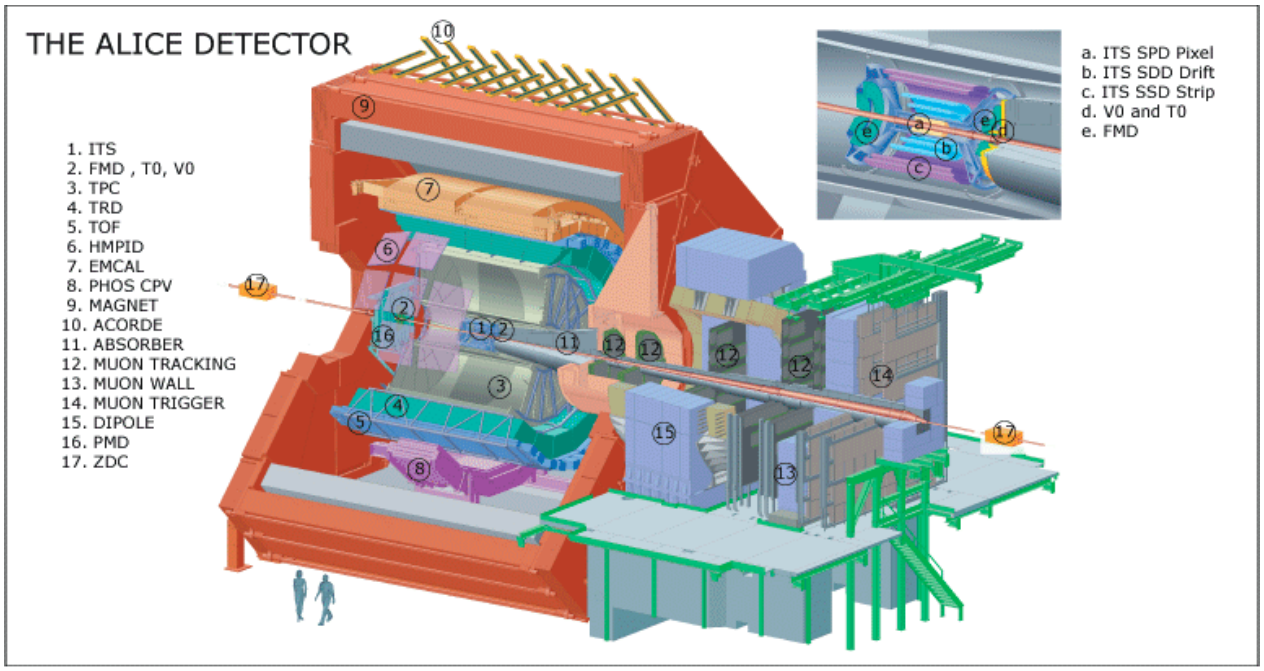

Figure 18: Schematic view of the ALICE detector and its subdetectors[17]

A.3 Code used in macro for charm-forced pp collision simulation

Note that in the code below, some histograms were saved which were eventually left out of this thesis.

```
#include "TSystem.h"
#include "TH1D.h"
#include "TH2D.h"
#include "TH3D.h"
#include "TClonesArray.h"
#include "TPythia8.h"
```

```
#include "TParticle.h"
#include "TDatabasePDG.h"
#include "TCanvas.h"
#include "THStack.h"
#include "TLegend.h"

void sim(Int_t nev  = 10000000, Int_t ndeb = 1)
{
   const char *p8dataenv = gSystem->Getenv("PYTHIA8DATA");
   if (!p8dataenv) {
      const char *p8env = gSystem->Getenv("PYTHIA8");
      if (!p8env) {
         Error("pythia8.C",
               "Environment variable PYTHIA8 must contain path to pythia directory!");
         return;
      }
      TString p8d = p8env;
      p8d += "/xmldoc";
      gSystem->Setenv("PYTHIA8DATA", p8d);
   }
   const char* path = gSystem->ExpandPathName("$PYTHIA8DATA");
   if (gSystem->AccessPathName(path)) {
         Error("pythia8.C",
               "Environment variable PYTHIA8DATA must contain path to $PYTHIA8/xmldoc directory !");
      return;
   }
// Load libraries
#ifndef G__WIN32 // Pythia8 is a static library on Windows
   if (gSystem->Getenv("PYTHIA8")) {
      gSystem->Load("$PYTHIA8/lib/libpythia8");
   } else {
      gSystem->Load("libpythia8");
   }
#endif
   gSystem->Load("libEG");
   gSystem->Load("libEGPythia8");



   //----------------------Histograms-ALICE-pseudorapidity-------------------------------------


   TH1D* ptPionH = new TH1D("ptpionH", "pion p_{t}", 10000, 0., 24);
   TH1D* ptPionLambdaH = new TH1D("ptpionlH", "pion from #Lambda_{c}  p_{t}", 10000, 0., 24);
   TH1D* ptLambdaH = new TH1D("ptLambda", "All #Lambda_{t} p_{t}", 100, 0., 24);
   TH1D* ptLambdaSigmaH = new TH1D("ptLambdacs", "#Lambda_{c} from #Sigma_{c} p_{t}"
                        , 10000, 0., 24);
   TH1D* ptSigmaH = new TH1D("ptSigmacH", "#Sigma_{c} p_{t}", 10000, 0., 24);
   TH1D* ptPionSigmaH = new TH1D("ptPionSigmaH","pion from #Sigma_{c} p_{t}", 10000, 0., 24);

   TH1D* ptps1 = new TH1D("ptp1","Pion p_{t} with #Sigma_{c} p_{t} [1-2 GeV/c]",10000, 0., 24);
   TH1D* ptps2 = new TH1D("ptp2","Pion p_{t} with #Sigma_{c} p_{t} [2-3 GeV/c]",10000, 0., 24);
   TH1D* ptps3 = new TH1D("ptp3","Pion p_{t} with #Sigma_{c} p_{t} [3-4 GeV/c]",10000, 0., 24);
   TH1D* ptps4 = new TH1D("ptp4","Pion p_{t} with #Sigma_{c} p_{t} [4-6 GeV/c]",10000, 0., 24);
   TH1D* ptps5 = new TH1D("ptp5","Pion p_{t} with #Sigma_{c} p_{t} [6-12 GeV/c]",10000, 0., 24);
   TH1D* ptps6 = new TH1D("ptp6","Pion p_{t} with #Sigma_{c} p_{t} [>12 GeV/c]",10000, 0., 24);

   TH3D* xyptPionSigmaH = new TH3D("xyptPionSigmaH","#pi_{soft} production location"
                        ,100, -100, 100, 100, -100, 100,100,0,24);

   TH2D* svspH = new TH2D("svspH", "#Sigma_{c} p_{t} v.s. soft pion p_{t}",10000,0,24,10000,0,5);


   //----------------------Variable-definitions-------------------------------------
   Float_t etamin = -0.9;
   Float_t etamax = 0.9;
```

```
   //-------------------------------------------------------------------------------------------


   //-------------------------------------------------------------------------------------------
// Array of all particles
   TClonesArray* particles = new TClonesArray("TParticle", 1000);
// Create pythia8 object
   TPythia8* pythia8 = new TPythia8();
// Configure
   pythia8->ReadString("HardQCD:all = on");
   pythia8->ReadString("HardQCD:gg2ccbar = on");
   pythia8->ReadString("HardQCD:qqbar2ccbar = on");
   pythia8->ReadString("phaseSpace:pTHatMin = 50.");
// Initialize
   pythia8->Initialize(2212 /* p */, 2212 /* p */, 10000. /* GeV */);
   //-------------------------------------------------------------------------------------------

   //----------------------event-loop-------------------------------------------------------------

 for (Int_t iev = 0; iev < nev; iev++) {
      pythia8->GenerateEvent();
      if (iev < ndeb) pythia8->EventListing();
      pythia8->ImportParticles(particles,"All");
      Int_t np = particles->GetEntriesFast();

// ------------------------------Partilce-loop-for-all-particles-----------------------------------

         for (Int_t ip = 0; ip < np; ip++) {
         TParticle* part = (TParticle*) particles->At(ip);
         Int_t pdg = part->GetPdgCode();
         Float_t pt  = part->Pt();
         Float_t vx = part->Vx();
         Float_t vy = part->Vy();
         Float_t eta = part->Eta();



         //Pion
         if (((pdg == 211) || (pdg == -211)) && (pt >= 0) && ((eta >= etamin)
            && (eta <= etamax))) ptPionH->Fill(pt);

         //Lambda_c
         if (((pdg == 4122) || (pdg == -4122)) && (pt >= 0) && ((eta >= etamin)
            && (eta <= etamax))) ptLambdaH->Fill(pt);

         //Sigma_c
         if (((pdg == 4112) || (pdg == -4112) || (pdg == 4222) || (pdg == -4222))
            && (pt >= 0) && ((eta >= etamin) && (eta <= etamax))) ptSigmaH->Fill(pt);

         //----------------------Particle-loop-for-particles-with-specific-mother-particle---------


         if ((!part) || part->IsPrimary()) continue;
         Int_t motherindex = part->GetFirstMother();
         TParticle* mpart = (TParticle*) particles->At(motherindex);
         Int_t mpdg = mpart->GetPdgCode();
         Float_t mpt = mpart->Pt();
         Float_t meta = mpart->Eta();

         //Pions with Lambda_c as mother-particle
         if (((pdg == 211) || (pdg == -211)) && (mpdg == 4122) && (pt >= 0)
            && ((eta >= etamin) && (eta <= etamax)) && ((meta >= etamin)
            && (meta <= etamax))) ptPionLambdaH->Fill(pt);

         //Lambda_c with Sigma_c as mother-particle
         if (((pdg == 4122) || (pdg == -4122)) && (pt >= 0) && ((mpdg == 4112)
            || (mpdg == -4112)) && ((eta >= etamin) && (eta <= etamax))
            && ((meta >= etamin) && (meta <= etamax))) ptLambdaSigmaH->Fill(pt);
```

```
        //Pion with Sigma_c as mother-particle
        if (((pdg == 211) || (pdg == -211)) && ((mpdg == 4112) || (mpdg == -4112)
           || (mpdg == 4222) || (mpdg == -4222)) && (pt >= 0) && ((eta >= etamin)
           && (eta <= etamax)) && ((meta >= etamin) && (meta <= etamax)))
           (ptPionSigmaH->Fill(pt), xyptPionSigmaH->Fill(vx,vy,pt), svspH->Fill(mpt,pt));

        //----------------------Particle-loop-for-pions-from-sigma_c-pt-at-different-pt-ranges-----

        if (((pdg == 211) || (pdg == -211)) && ((mpdg == 4112) || (mpdg == -4112)
           || (mpdg == 4222) || (mpdg == -4222)) && ((mpt >= 1) && (mpt <=2))
           && ((eta >= etamin) && (eta <= etamax)) && ((meta >= etamin)
           && (meta <= etamax))) (ptps1->Fill(pt));
        if (((pdg == 211) || (pdg == -211)) && ((mpdg == 4112) || (mpdg == -4112)
           || (mpdg == 4222) || (mpdg == -4222)) && ((mpt >= 2) && (mpt <=3))
           && ((eta >= etamin) && (eta <= etamax)) && ((meta >= etamin)
           && (meta <= etamax))) (ptps2->Fill(pt));
        if (((pdg == 211) || (pdg == -211)) && ((mpdg == 4112) || (mpdg == -4112)
           || (mpdg == 4222) || (mpdg == -4222)) && ((mpt >= 3) && (mpt <=4))
           && ((eta >= etamin) && (eta <= etamax)) && ((meta >= etamin)
           && (meta <= etamax))) (ptps3->Fill(pt));
        if (((pdg == 211) || (pdg == -211)) && ((mpdg == 4112) || (mpdg == -4112)
           || (mpdg == 4222) || (mpdg == -4222)) && ((mpt >= 4) && (mpt <=6))
           && ((eta >= etamin) && (eta <= etamax)) && ((meta >= etamin)
           && (meta <= etamax))) (ptps4->Fill(pt));
        if (((pdg == 211) || (pdg == -211)) && ((mpdg == 4112) || (mpdg == -4112)
           || (mpdg == 4222) || (mpdg == -4222)) && ((mpt >= 6) && (mpt <=12))
           && ((eta >= etamin) && (eta <= etamax)) && ((meta >= etamin)
           && (meta <= etamax))) (ptps5->Fill(pt));
        if (((pdg == 211) || (pdg == -211)) && ((mpdg == 4112) || (mpdg == -4112)
           || (mpdg == 4222) || (mpdg == -4222)) && (mpt >= 12) && ((eta >= etamin)
           && (eta <= etamax)) && ((meta >= etamin) && (meta <= etamax))) (ptps6->Fill(pt));

    }
}

//----------------------Saving-Histograms-to-root-file-----------------------------------------

  TFile *MyFile = new TFile("data10Mrebinforced.root","NEW");
  gFile = MyFile;

  ptPionH->Write();
  ptPionLambdaH->Write();
  ptPionSigmaH->Write();
  ptLambdaH->Write();
  ptLambdaSigmaH->Write();
  ptSigmaH->Write();
  ptps1->Write();
  ptps2->Write();
  ptps3->Write();
  ptps4->Write();
  ptps5->Write();
  ptps6->Write();
  xyptPionSigmaH->Write();
  svspH->Write();

  MyFile->Close();

}
```